Multi-Objective Design Optimization of a Hybrid Excitation Flux Switching Permanent Magnet Motor Based on Design Sensitivity Analysis

Behrooz Rezaeealam[1*], Farhad Rezaee-Alam[2], and Javad Rahmani Fard[3]

[1] Departement of Electrical Engineering, Lorestan University, 68151-44316, Khorramabad, Lorestan, Iran, +989163988261, rezaee.bh@lu.ac.ir

[2] Departement of Electrical Engineering, Lorestan University, 68151-44316, Khorramabad, Lorestan, Iran, +989166591727, rezaee.fa @lu.ac.ir

[3] Departement of Electrical Engineering, Arak University of Technology, 38181-46763, Arak, Iran, +989120517088, javad.rahmani.fard@gmail.com

Abstract

The hybrid excitation flux switching permanent magnet (HEFSPM) motor with magnetic bridge is a topology of hybrid excitation flux-switching PM machines. Despite its excellent performance such as high torque/power density, high flux enhancing/weakening capability and so on, it has received less attention due to its complicated structure. Therefore, its optimal design and performance all need to be further investigated. This paper presents a multi objective optimization design of a HEFSPM motor with magnetic bridge based on design sensitivity analysis. At first, the machine structure and basic working principle are discussed briefly. Then, a design sensitivity analysis for geometric optimization is carried out to improve the motor performance. This optimized motor is compared with initial design. Finally, a prototype of the optimized proposed motor is built and tested to validate the simulation results.

Index Terms: Cogging torque, Finite Element Method (FEM), Flux-switching, Hybrid excitation, Magnetic bridge, Permanent Magnet (PM).

1. Introduction

The flux switching PM motor (FSPM) has many advantages, such as no PMs or excitation windings on the rotor, the simple rotor with high mechanical strength. Moreover, the PMs are located in the stator, which is convenient for heat dissipation and cooling. Besides, the stator flux is bipolar, and the power density is relatively high [1-4]. On the other hand, its magnetic field is hard to adjust [5]. The electric excitation flux switching motor uses an electric excitation structure instead of PMs.

The magnetic flux switching of the electric excitation structure can realize the adjustment of the main magnetic field and overcome the shortcomings of the difficulty of PM magnetic field

adjustment. With reasonable adjustment of the DC excitation current, the motor can run in a wide range of speed. But the common problems of electric excitation structure are large excitation loss, low torque density and low efficiency [6-8]. In order to improve the magnetization ability of PM flux switching motors and maintain high torque density, hybrid excitation flux switching PM (HEFSPM) motors are proposed [9-18].

The first two types of HEFSPM motors reduce the volume of PMs and add DC excitation windings in the vacated areas [9-11] (Figure 1). With the excitation current changes, the function of adjusting the main magnetic field of the motor can be realized and the motor can work in a wide speed range. However, the problem faced by this structure is that the electric excitation magnetic flux passes through the PM, which is equivalent to an air gap and has large magnetic circuit reluctance, and has limited adjustment capabilities. There is also a problem of PM demagnetization.

Figure 1

Therefore, a HEFSPM motor with a magnetic bridge structure is proposed [12-13]. This solves the problem of small electric excitation magnetic flux, and at the same time, the risk of demagnetization is improved. However, due to the existence of the magnetic bridge, a shorted magnetic circuit is provided for the PMs, and an excessively wide magnetic bridge will greatly reduce the utilization rate of the PMs. Therefore, the efficiency of electric excitation and the utilization of PMs are contradictory when there is a magnetic bridge. This can also provide us with an entry point for research. In [14-15], the E-core HEFSPM motor is presented (Figure 2(a)). In this structure, a DC excitation winding structure is added to the middle teeth of the E-shaped iron core. This hybrid excitation structure can prevent PMs from shorting the magnetic circuit. However, there are also the problems of large magnetic resistance, large excitation loss, and unsatisfactory magnetic field adjustment ability of the electric excitation magnetic circuit.

Therefore, the existence of electric excitation winding will inevitably reduce the armature slot area and the torque density of the motor. A parallel HEFSPM motor was presented in [16] (Figure 2(b)). One section adopts electric excitation structure and one section adopts PM excitation structure. This structure can not only avoid the short magnetic circuit of PMs, but also improve the utilization rate of PMs and maintain high magnetic field adjustment capability. On the other hand, the motor has a large volume and a relatively low torque density and a complex structure. In [17-18], one HEFS motor was proposed as a variable flux motor which has better

efficiency only at light-load and high-speed operating region (Figure 2(c))

Figure 2

In [19], an archive-based multi-objective genetic algorithm optimization based on the sensitivity analysis is presented for a double stator hybrid-excitation flux-switching PM motor. The multi-objective optimization has been divided into three steps, which are optimization of the stator and rotor diameter, optimization of the inner stator and optimization of the outer stator. Every optimization step has different objective functions. In [20], a 6/22-p outer-rotor V-shaped PM Flux Switching motor was designed with the multi-level method. The parameters were classified into two level according to their order of sensitivities: less-important parameters and more-important parameters. The more-important parameters were optimized by design of experiment and response surface methodology and the less-important parameters were optimized individually. A modular hybrid-excitation FSPM machine has been presented in [21] to increase PM usages. Moreover, a multi-objective optimization is conducted based on response surface method and sequential non-linear programming method. In [22] a multi-excitation flux switching motor is presented. The hybrid-PMs of rare-earth Nd-Fe-B and non-rare earth ferrite are used to decrease the utilization of rare-earth PM material. Moreover, the multi-objective optimization is done by genetic algorithm and response surface methodology.

This paper investigated a three-phase 12/10-poles hybrid excitation flux switching motor with the magnetic bridge structure. The existence of the magnetic bridge improves the ability of magnetic field regulation. As an important structure of HEFSPM motor, there are relatively few related researches at present. In this paper, the geometric design optimization of the proposed motors is obtained by the design sensitivity analysis to reduce the cogging torque and increase the average torque. The influence of the change of the structure parameters on the performance is analyzed. Finally, based on the optimization results, an experimental prototype motor is manufactured and tested.

2. MACHINE STRUCTURE AND BASIC WORKING PRINCIPLE OF HEFSPM MOTOR

A. Machine structure

Figure 3 demonstrates the topology of the HEFSPM with the magnetic bridge. DC excitation windings are installed in the bottom of PMs. Outside of the excitation winding slots are

connected by a magnetic bridge. Each PM in the stator has a DC excitation magneto motive force (MMF), whose size and direction change with the change of the excitation current to achieve the purpose of adjusting the main magnetic field. The stator core of the hybrid excitation flux switching motor is a whole, which is conducive to the installation of the motor.

Figure 3

B. Basic Working Principle

The basic working principle of regulating the magnetic field can be explained as follows:

(1). PMs work alone

Figure 4(a) illustrates the magnetic flux paths at this condition. As can be seen, the amount of PM flux passing through the short-circuit path and magnetic bridge is greater than that of passing through the air gap.

(2). Electrical excitation works alone

Figure 4(b) illustrates the magnetic flux paths when electrical excitation works alone. As can be seen, most of the excitation flux passes through the air-gap, since the reluctance of PM is much higher than that of the stator. Hence the flux paths can be controlled by changing the direction and amplitude of the electrical excitation current.

(3). Two magnetic potential sources work together

When two magnetic potential sources work together, the flux paths are shown in Figure 4 (c). In

Figure 4 (c), the two magnetic potential are in the same direction. The flux linkage of armature windings is the sum of the fluxes generated by both magnetic potential sources. In the same direction, the air-gap flux density will be enhanced and in the opposite direction, air-gap flux density will be weakened and a wide speed range is achieved

Figure 4

The no-load magnetic field distribution in no-excitation current condition is shown in Figure 5. Figure 5(a)-(b) show field distribution at maximum positive flux linkages position and maximum negative flux linkages position, respectively. As can be seen, the amount of PM flux passing through the short-circuit path is greater than that of passing through the air gap. When two magnetic potential sources work together, the flux paths are shown in Figure 6(a)-(b). Two magnetic potential are in the same direction in Figure 6(a) and in the opposite direction in Figure 6(b). The flux linkage of armature windings is the sum of the fluxes generated by both

magnetic potential sources. In the same direction, the air-gap flux density will be enhanced and in the opposite direction, air-gap flux density will be weakened and a wide speed range is achieved.

Figure 5

Figure 6

3. DESIGN OF HEFSPM MOTOR

A. Initial design

The specifications of the investigated motor are shown in Table 1. The HEFSPM inherits the basic magnetic circuit characteristics of FSPM motor in its structure. Therefore, the power size equation in a FSPM motor can be used for a HEFSPM motor. So, the stator inner diameter can be expressed as [23]

$$D_a = \sqrt[3]{\frac{p_2}{\frac{\sqrt{2}\pi^3}{120}\times\frac{N_r}{N_s}\times k_d \times A_s \times B_g \times k_{fe} \times n \times c_s \times \eta}} \tag{1}$$

where N_s and N_r are stator and rotor pole numbers, respectively, P_2 is the output power, k_d is the magnetic flux leakage coefficient, A_s is the electrical loading, B_g is the magnetic loading, k_{fe} is the split ratio ($k_{fe}=l_a/D_a$), l_a is the length of the motor core, n is the rotor speed in *rpm*, c_s is the stator tooth arc coefficient, η is the efficiency of motor. In [24], a simple analytical method was developed to optimize the combination of stator and rotor pole numbers for the FSPM machines. In summary, the 12s-10p is a conventional combination of a flux switching PM motors that can induce symmetrical and balanced three-phase back-EMF waveforms. Refer to the design data of FSPM motor, after repeated calculation and comparison, take k_d =0.9, A_s =14000 *A*/*m*, B_g=1.5 T, η=0.85, k_{fe}=0.6 and c_s=0.25. Combining the relevant values in Table 1, the initial stator inner diameter of the HEFSPM motor D_a= 62 *mm* can be obtained

Table 1

According to the relationship between the back EMF and the phase flux linkage, the number of turns of the phase winding will be derived as

$$N_{ph} = \frac{E_m}{\omega_r \times N_r \times k_d \times B_g \times l_a \times \frac{\pi D_a}{N_s} \times c_s} \tag{2}$$

where E_m is the amplitude of the no-load back EMF. To determine E_m, use the following equation as [23]:

$$P_{out} = \eta \times P_{in} = \eta \times 3 \times \frac{E_m}{\sqrt{2}} \times \frac{I_m}{\sqrt{2}} \tag{3}$$

where P_{in} and P_{out} are the input power and output power, respectively. Therefore, E_m can be written as

$$E_m = \frac{2P_{out}}{3\eta \times I_m} \tag{4}$$

According to (2) and (4), the number of turns of each phase is 76.56. Because each phase consists of 4 coils, the number of turns of each phase must be a multiple of 4. Therefore, we consider the number of turns to be 80.

The rotor tooth width $b_{rt}(\theta_{rt})$, the stator tooth width $b_t(\theta_t)$, PM width $h_{pm}(\theta_{pm})$, armature winding slot width $b_s(\theta_s)$, stator pole pitch $b_{s\tau}(\theta_{\tau s})$, satisfy the following relationships:

$$b_t = h_{pm} = b_s = \frac{\pi D_a}{4N_s} \tag{5}$$

$$\theta_{st} = 2\theta_t + \theta_{pm} + \theta_s = \frac{2\pi}{N_s}$$

So, here b_t=h_{pm}=b_s=4.1mm. The rotor parameter that has a greater impact on the performance of the motor is the rotor pole arc width. In the initial design, take the rotor pole arc coefficient k_r =0.33 and b_{rt}=6.2mm. The rotor pole height is about 20 times the air gap length referring to the design method of the switched reluctance motor. The thickness of the rotor yoke is about 0.6-0.8 of rotor pole width [25].

Figure 7

B. Design of electric excitation MMF

Many involved parameters, including the radial height of the PM, w_{pm}, the width of the magnetic bridge, w_b, the width of the core in the middle of the electric excitation slot, w_e, the thickness of the stator yoke, b_e, are shown in Figure 7.

According to magnetic circuit model presented in [20] and the definition of magnetic flux, the maximum magnetic flux of phase *A* is obtained as

$$\phi_A = k_d \times B_g \times l_{fe} \times \frac{\pi D_a}{N_s} \times c_s = \frac{2F_e}{R_g} \tag{6}$$

where F_e is MMF of electric excitation and R_g is the air-gap reluctance. From above equation, ϕ_A is about 15mWb. Assuming that the radial length of the air-gap g= 0.5 mm, F_e=960 $A.T$ can be estimated.

C. *PM Design*

Generally, when the electric excitation is not energized, the magnetic flux density at the magnetic bridge is designed at the knee point of the magnetization curve, i.e. B_{mb}= 1.8T. The thickness of the magnetic bridge is w_b=(0.6~1)b_t and we take w_b=2.5mm. The width of the core in the middle of the electric excitation slot w_e=(2~3)w_b and we take w_e=6.3mm. The thickness of the stator yoke is generally b_e= (0.8~1)b_t and we take b_e=4mm.

After determining the radial thickness of the PM, other dimensions can be determined. At this time, the selection of the initial magnetic flux density of the air gap B_{g_org} is involved.

When the value of B_{g_org} is large, it means that the electric excitation adjustment range will not be too large. When the value of B_{g_org} is small, it means that the electric excitation is not working and the magnetic loading is quite low and the torque density will not be very high. Here choose B_{g_org}=0.4B_g, i.e B_{g_org}=0.6T. When the initial magnetic flux density of the air gap is determined, a one-dimensional linear equation about the thickness of the PM may write as

$$\phi_A = k_d \times B_{g-org} \times l_a \times \frac{\pi D_a}{N_s} \times c_s = \frac{2F_{pm} \times R_b}{\left(R_{pm} + R_b\right)R_g + R_{pm} \times R_b} \tag{7}$$

where R_{pm} is the PM reluctance, R_b is the reluctance of the magnetic bridge. From above equation, the radial thickness of the permanent magnet can be determined to be w_{pm}=8 mm, and all the parameters of the motor can be determined basically.

4. GEOMETRICAL PARAMETERS REFINEMENT

Geometrical parameters refinements using design sensitivity analysis (DSA) are carried out to reduce cogging torque and improve back-EMF of HEFSPM machine. The analysis is conducted by the finite element method (FEM). This method is discussed in [19]. Table 2 shows the variables and definitions of the motor. Figure 8 sums up the steps of the DSA of the motor

Table 2

Figure 8

1) PM thickness

Ensure that the armature slot width θ_s is unchanged, i.e, $2\theta_t+\theta_{pm}=3\pi/2N_s$. We define the coefficient $k_{pm}=\theta_{pm}/\theta_{pm\text{-}ort}$, $\theta_{pm\text{-}ort}$ is the initial PM thickness, and $\theta_{pm\text{-}rt}=2\pi/12/4=7.5^{\circ}$. As shown in Figure 9(a) and Figure 9(b), the change in PM thickness not only affects the amplitude of the cogging torque but also changes the phase of the cogging torque. When $k_{pm}>1$ and $k_{pm}<1$ the cogging torque increases and the cogging torque is the smallest under the initial size, i.e $k_{pm}=1$. As shown in Figure 9(c) and Figure 9(d), the change in PM thickness not only affects the amplitude of the back EMF, but also increases the high-order harmonics to distort the back-EMF waveform. Excessively wide PMs narrow the width of the stator teeth and increase the reluctance in the main magnetic circuit. So the no-load magnetic flux and the back-EMF amplitude will decrease. If the PM is too narrow, the volume of the PM is reduced, and the magnetic flux generated by the PMs is reduced. So the amplitude of the back EMF will also decrease, and it will also cause the risk of PM demagnetization. It can be seen from the Figure 9(d) that the fundamental wave amplitude of the back-EMF is the largest when $k_{pm}=0.65$, and the amplitude of the back-EMF is slightly reduced when $k_{pm}=0.8$, but the 5th and 7th harmonics are significantly reduced when $k_{pm}=0.8$.

Figure 9

Figure 10

Figure 10 shows the effect of changes in excitation current on the no-load flux linkage amplitude. As can see, in the low excitation current density area (Je=0~3A/mm2), the smaller thickness of the PM, the smaller amplitude of the initial flux linkage in the winding. This is because the MMF of the PM is small and the PM flux generated is less, and the magnetic flux mainly flows through the magnetic bridge. In the medium excitation current density area (J_e=3A/mm2~7A/mm2), it can be seen that when the thickness of the PM is small, the slope of the no-load flux linkage amplitude is large. This characteristic is very good, because it means that a smaller excitation current can obtain a larger no-load magnetic flux, which is beneficial to increase the output torque of the motor.

In the area of high excitation current density (J_e=7A/mm^2), as the excitation current density increases, the growth rate of the magnetic link amplitude becomes slower, or even declines, and the smaller the thickness of the PM, the stronger this trend. There are two reasons for this

phenomenon: (1) the increase in the amplitude of the no-load flux linkage causes local saturation of the stator teeth. So the slope of the change in the amplitude of the magnetic flux reduces, (2) the increase in the MMF of the electric excitation changes the operating point of the PM, and the ability of the PM to generate magnetic flux and even demagnetization occurs. Therefore, in order to obtain a higher tuning range, it is necessary to comprehensively consider the effect of electric excitation and the demagnetization of PMs.

2) Stator slot width

As shown in Figure 11(a)-(b), it can be seen that the change of the stator slot width cannot change the phase of the cogging torque, but only the amplitude. The amplitude of the cogging torque increases with the decrease of the slot. When the slot width decreases to a certain value, the cogging torque begins to decrease again. The peak-to-peak cogging torque reaches 0.4 N.m when the slot width b_s=1.25 mm.

Compared with the original size, the cogging torque increased by 2 times. As shown in Figure 11(c)-(d), the change in the width of the stator slot not only affects the amplitude of the back-EMF, but also increases the high-order harmonics to distort the back-EMF waveform. The harmonic analysis shows that when the slot width is reduced to b_s=1.25 mm, the fundamental wave amplitude of the back EMF is 20.8V i.e. 10% higher than the initial size of 18.6V. On the whole, the narrowing of the slots will increase the amplitude of other higher harmonics. It can be seen that the 5th and 7th harmonics in the back EMF are more obvious.

Figure 11

3) Rotor pole width

As shown in Figure 12 (a)-(b), the rotor pole arc coefficient k_r=0.2~0.5, and the cogging torque of the motor is obtained. It can be seen that the rotor pole width affects the amplitude and When k_r=0.35, the cogging torque reaches a small value, and the rotor pole width at this time is exactly the same as the rotor pole width of the initial size. If the rotor pole width is too narrow, the overlap area between the stator teeth and the rotor pole becomes smaller, and the magnetic resistance in the main magnetic circuit becomes larger. The rotor poles are closed to form leakage flux, which causes the back EMF to decrease.

As shown in Figure 12 (c)-(d), the harmonic analysis shows that when k_r = 0.4, the fundamental wave amplitude of the back-EMF is the largest, and the 5th harmonic is smaller. If the rotor pole is too wide or too narrow, it will cause the increase of the 5th harmonic in the

back-EMF, and the other harmonics will remain basically unchanged.

Figure 12

4) Magnetic bridge width

The size and direction of the magnetic flux density at the stator magnetic bridge directly affects the electric excitation's ability to adjust the main magnetic flux. Figure 13 shows the optimization analysis of the magnetic bridge width. When w_b=0.5*mm* the magnetic tuning range is extremely small, and it is basically equivalent to a FSPM motor without a magnetic bridge structure. Therefore, the width of the magnetic bridge should not be too narrow. When the width of the magnetic bridge is increased, the initial magnetic flux passing through the air gap will decrease sharply. When w_b=4.5*mm*, if the excitation current is not applied, the motor's magnetic load is very small and the torque output capacity is very small.

Figure 13

When the electric excitation current is applied, the no-load flux linkage amplitude increases quickly, and the magnetic flux amplitude follows the excitation. Moreover, the current density changes approximately linearly, which is beneficial to the magnetization performance of the motor. However, the use of a too wide magnetic bridge will affect the area of the field winding slot, and the maximum value of the flux linkage will not become larger due to the increase in the width of the magnetic bridge.

5) The width of the core in the middle of the excitation slot

The iron core in the middle of the field winding slot is the main path which the electric excitation magnetic flux will pass. When the electric excitation current is zero, the short circuit magnetic circuit of two adjacent permanent magnets flows through the middle iron core, so the width of the iron core should be wider than the magnetic bridge, generally should be about 2 times. As shown in Figure 14, when the core is too narrow, the initial flux linkage amplitude of the winding will be too high, can cause the induction voltage to rise excessively and damage the motor. When the core is too wide, it will seriously affect the slot area of the electric excitation winding, which will cause difficulties in the design of the excitation current and also affect the tuning range.

Figure 14

6) The width of the stator yoke

The stator yoke is the common part of the excitation magnetic circuit and the armature reaction

magnetic circuit, so the width of the stator yoke not only affects the magnetization range of the motor, but also affects the armature reaction and output torque of the motor, as shown in Figure 15. As the stator yoke becomes wider, the initial magnetic flux amplitude of the motor becomes smaller, which is beneficial to the magnetization range of the motor, but the stator yoke should not be too wide, which will affect the armature slot area.

Figure 15

Table 3 shows the optimized values by DSA.

Table 3

Figure 16(a)-(b) show the results of a comparison between the initial design and the optimal design by the DSA method. As can be seen, in the optimal design, the ability to flux weakening and flux enhancing has been significantly improved.

Figure 16

Figure 16(c)-(d) show a comparison of cogging torque and back-EMF in these motors. As can be seen, the cogging torque has been reduced by about 80% and the back-EMF waveform has become more sinusoidal.

Additionally, the results of d/q axes inductances, efficiency and power factor before and after optimization are compared and listed in Table 4.

Table 4

5. EXPERIMENTAL VALIDATIONS

The optimized HEFSPM machine with magnetic bridge is fabricated to validate the foregoing analyses. The stator and rotor lamination and experimental setup are shown in Figure 17.

A 1 kW separately excited DC machine is coupled with HEFSPM machine. When measuring the back-EMF of the HEFSPM motor, the DC machine is used as a motor. Figure 17(c) shows the cogging torque test equipment (ONO SOKKI TS-700), which is used to measure the cogging torque of the motor.

Figure 17

The electromagnetic performance of the fabricated motor is predicted by the 2-D FE method and also measured. Figure 18 presents the cogging torque of the motor. As seen, the FE and experimental results are in very good agreement.

Figure 18

Figure 19(a) shows the back-EMF at rated speed for AT=-960, 0 and +960 at 1200 *r/min*. It can be seen that the back-EMF obtained by the two research methods are relatively close. Define the motor voltage regulation as $V.R\%=((E_m/E_{m0})-1)\times 100$, where E_m and E_{m0} are the peak value of back-EMF with electric excitation and without electric excitation, respectively. Figure 19(b) shows the voltage regulation of the motor obtained from the 2-D FEM and the measured data of the prototype motor when the MMF of the electric excitation changes from - 960A.T to +960A.T at 1200 *r/min*. In the optimized motor, the flux-weakening capability is lower than the flux-enhancing capability, since the flux- enhancing MMF decreases the magnetic saturation in the stator teeth, while the flux- weakening MMF increases the magnetic saturation

Figure 19

6. CONCLUSION

An optimal hybrid-excitation FSPM motor with magnetic bridge has been presented and analyzed. Geometrical refinements of the initial design motor were carried out using a design sensitivity analysis based on the FEM to improve machine performance. A comparison the initial design and the optimal design by the DSA method, shows that optimized structure has advantages in increasing the magnetization range of the motor, increasing the output torque and reducing the cogging torque of the permanent magnet. From the FEM results and measured data it can be found, that the influence of the electric excitation MMF on the voltage regulation is nonlinear

References

[1] Hao, C., EL-Refaie, A. M., and Demerdash, N. A. O. "Flux-switching permanent magnet machines: a review of opportunities and challenges-part I: fundamentals and topologies.", IEEE Trans. Energy Conver., **35**(2), pp.684-698, (2019).

[2] Zhu, X., Hua, W., and Zhang, G. "Analysis and reduction of cogging torque for flux switching permanent magnet machines", IEEE Trans. Ind. Appl., **55**(6), pp.5854-5864, (2019).

[3] Chen, Y., and Zhou, Y. "Radial displacement sensorless control of bearingless flux switching permanent magnet machines based on difference of symmetric-winding flux linkages.", IEEE Trans. Ind. Electron., **68**(9), pp.7793-7803, (2020).

[4] Zhu, J., Wu, L., and Wen, H. "Optimization and comparison of dual-armature flux switching permanent magnet machines with different stator core shapes." IEEE Trans. Ind. Appl., **58**(1), pp.314-324, (2022).

[5] Yu, D., Yunyun, C., Jiahong, Z., and et al. "Design and performance investigation of double-side hybrid excitation flux-switching machine." IEEE International Conference on Applied Superconductivity and Electromagnetic Devices (ASEMD), China, (2018).

[6] Tang, Y., Paulides, J. J. H., Motoasca, T. E., and et al. "Flux-switching machine with DC excitation", IEEE Trans. Magn., **48**(11), pp. 3583-3586, (2012).

[7] Wang, Y., and Deng, Z. Q., "Analysis of electromagnetic performance and control schemes of electrical excitation flux-switching machine for DC power systems", IEEE Trans. Energy Conver., **27**(4), pp. 844-855, (2012).

[8] Wang, Y., and Deng, Z. "An integration algorithm for stator flux estimation of a Direct torque-controlled electrical excitation flux-switching generator" IEEE Trans. Energy Conver., **27**(2), pp. 411-420, (2012).

[9] Hua, W., Cheng, M., Zhang, G. "A novel hybrid excitation flux-switching motor for hybrid vehicles", IEEE Trans. Magn., **45**(10), pp. 4728-4731, (2009).

[10] Owen, R. L., Zhu, Z. Q., and Jewell, G. W., "Hybrid-excited flux-switching permanent-magnet machines with iron flux bridges", IEEE Trans. Magn., **46**(6), pp. 1726-1729, (2010).

[11] Hua, W., Zhang, G., Cheng, M.: "Flux-regulation theories and principles of hybrid-excited flux-switching machines", IEEE Trans. Ind. Electron., **62**(9), pp. 5359-5369, (2015).

[12] Nasr, A., Hlioui, S., Gabsi, M., et al.: "Design optimization of a hybrid excited flux switching machine for aircraft-safe DC power generation using a diode bridge rectifier", IEEE Trans. Ind. Electron., **64**(12), pp. 9896-9904, (2017).

[13] Abd Rani, J., Sulaiman, E., Ahmad, M. Z. and et al. "The Rotor-Stator Study of E-Core Hybrid Flux Switching Motor." Journal of Telecommunication, Electronic and Computer Engineering (JTEC), **10**(2), pp. 21-25, (2018).

[14] Ullah, W., Khan, F., Sulaiman, E., and et al. "Analytical validation of novel consequent pole E-core stator permanent magnet flux switching machine", IET Electr. Power Appl., **14**(5), pp. 789-796, (2020).

[15] Li, J., Wang, K., and Liu, C. "A novel E-core hybrid-excited flux switching machine based on biased flux", 20th International Conference on Electrical Machines and Systems (ICEMS), Australia, (2017).

[16] Li, X., Shen, F., Yu, S., and et al. "Flux-regulation principle and performance analysis of a novel axial partitioned stator hybrid-excitation flux-switching machine using parallel magnetic circuit", IEEE Trans. Ind. Electron., **68**(8), pp. 6560-6573, (2021).

[17] Okada, T., Matsumori, H., Kosaka, T., and et al. "Hybrid excitation flux switching motor with permanent magnet placed at middle of field coil slots and high filling factor windings", CES Transactions on Electrical Machines and Systems, **3**(3), pp. 248-258, (2019).

[18] Otsuka, K., Okada, T., Mifune, T., and et al. "Basic study on efficiency improvement of hybrid excitation flux switching motor using variably magnetizable permanent magnets for automotive traction drives", IEEE Energy Conversion Congress and Exposition (ECCE), USA, (2020).

[19] Hwang, C. C., Li, P. L., and Liu, C. T. "Design and analysis of a novel hybrid excited linear flux switching permanent magnet motor", IEEE Trans. Magn., **48**(11), pp. 2969-2972, (2012).

[20] Xu, Z., Xie, S., and Mao, P., "Analytical design of flux-switching hybrid excitation machine by a nonlinear magnetic circuit method", IEEE Trans. Magn., **49**(6), pp. 3002-3008, (2013).

[21] Yu, J., and Liu, C. "Multi-Objective Optimization of a Double-Stator Hybrid-Excited Flux-Switching Permanent-Magnet Machine", IEEE Trans. Energy Conver., **35**(1), pp. 312-323, (2020).

[22] Zhu, X., Shu, Z., Quan, L., and et al. "Multi-Objective Optimization of an Outer-Rotor V-Shaped Permanent Magnet Flux Switching Motor Based on Multi-Level Design Method", IEEE Trans. Magn., **52**(10), Article Sequence Number: 8205508, (2016).

[23] Hua, W., Cheng, M., Zhu, Z. Q., and et al. "Design of flux-switching permanent magnet machine considering the limitation of inverter and flux-weakening capability", Conference Record of the 2006 IEEE Industry Applications Conference Forty-First IAS Annual Meeting, USA, (2006).

[24] Chen, J. T., and Zhu, Z. Q., "Winding configurations and optimal stator and rotor pole combination of flux-switching PM brushless AC machines", IEEE Trans. Energy Conver., **25**(2), pp. 293-302, (2010).

[25] Krishnan R. "Switched reluctance motor drives: modeling, simulation, analysis, design, and applications", CRC press, (2017).

Behrooz Rezaeealam received the B.S. degree from Isfahan University of Technology in 1997, the M.S. and Ph.D. degrees from University of Tehran in 2000 and 2005, respectively, all in electrical engineering. He is currently an associate professor in the department of electrical engineering, Lorestan University, Iran. His research interests include modeling and design using FEM, electrical machines and drives.

Farhad Rezaee-Alam received the B.S. degree from Shahid Chamran University of Ahwaz in 2007, the M.S. and Ph.D. degrees from Khajeh Nasir University of Technology in 2010 and 2015, respectively, all in electrical engineering. He is currently an assistant professor in the department of electrical engineering, Lorestan University, Iran. His research interests include design and modeling of electric machines.

Javad Rahmani Fard received the B.S. degree from Shahed University, Tehran, Iran, in 2009, and the M.S. and Ph.D. degrees in electrical engineering from the K.N. Toosi University of Technology, Tehran, in 2012 and 2018, respectively. Currently, he is an assistant professor of the electrical engineering at Pooyesh Institute of Higher Education, Qom, Iran. His research interests include the analysis and design of electrical machines, and sensor-less variable-speed drives, multiphase variable-speed drives.

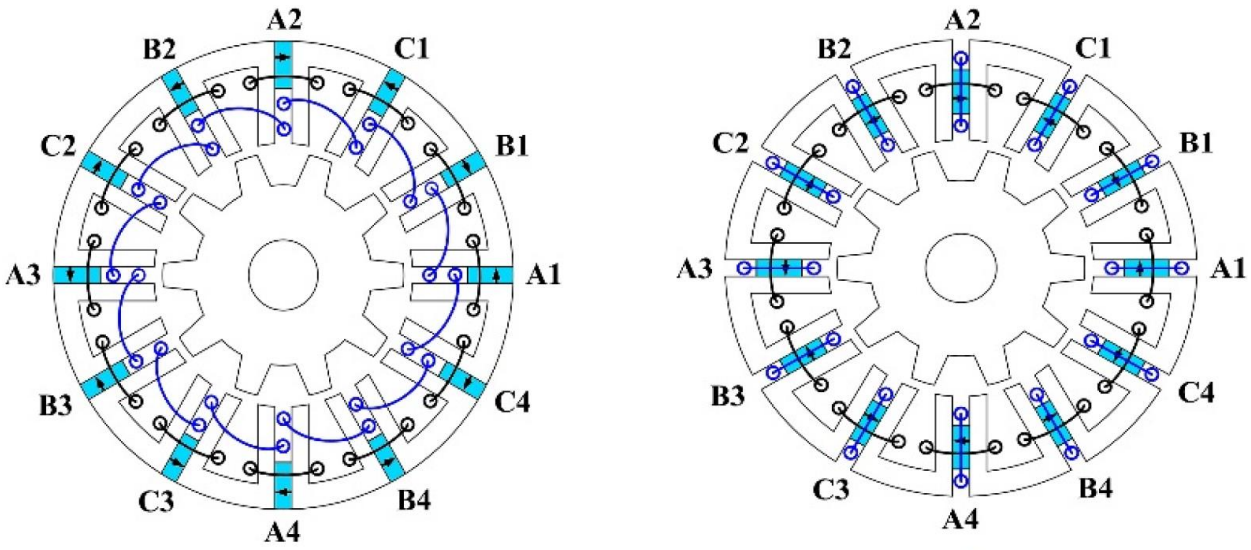
A2
B2
C1
C2
B1
A3
A1
B3
C4
C3
B4
A4
(a)
A2
B2
C1
C2
B1
A3
A1
B3
C4
C3
B4
A4
(b)

Figure 1

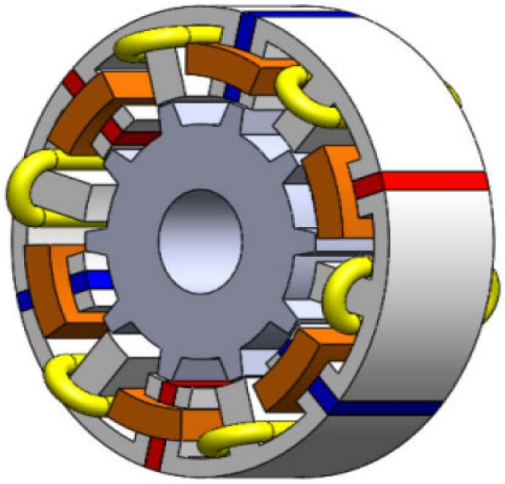

(a)

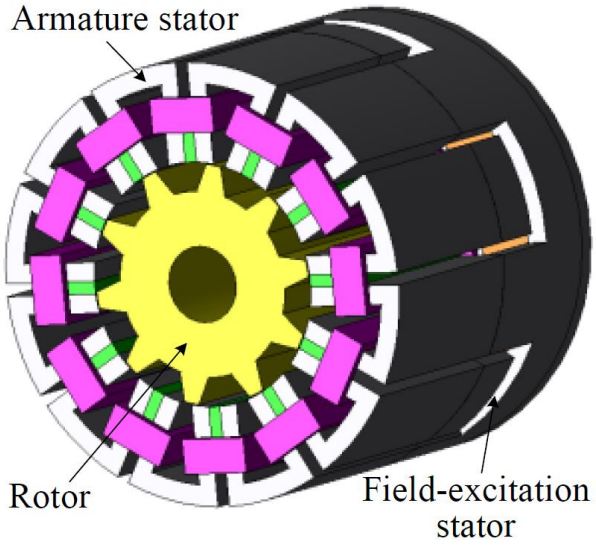
Armature stator
Rotor
Field-excitation stator

(b)

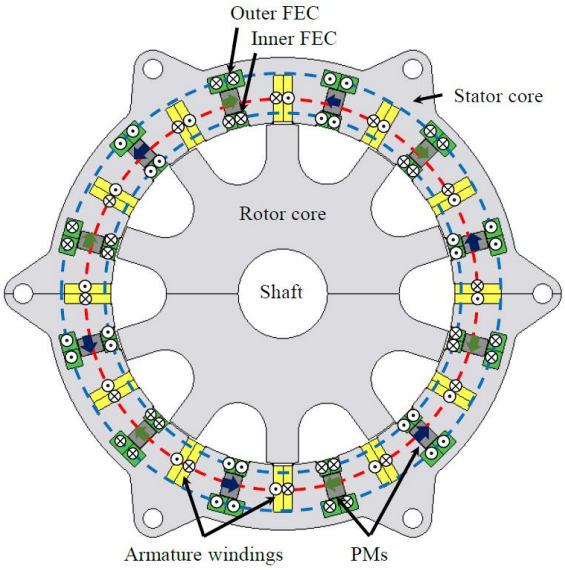
Outer FEC
Inner FEC
Stator core
Rotor core
Shaft
Armature windings
PMs

(c)

Figure 2

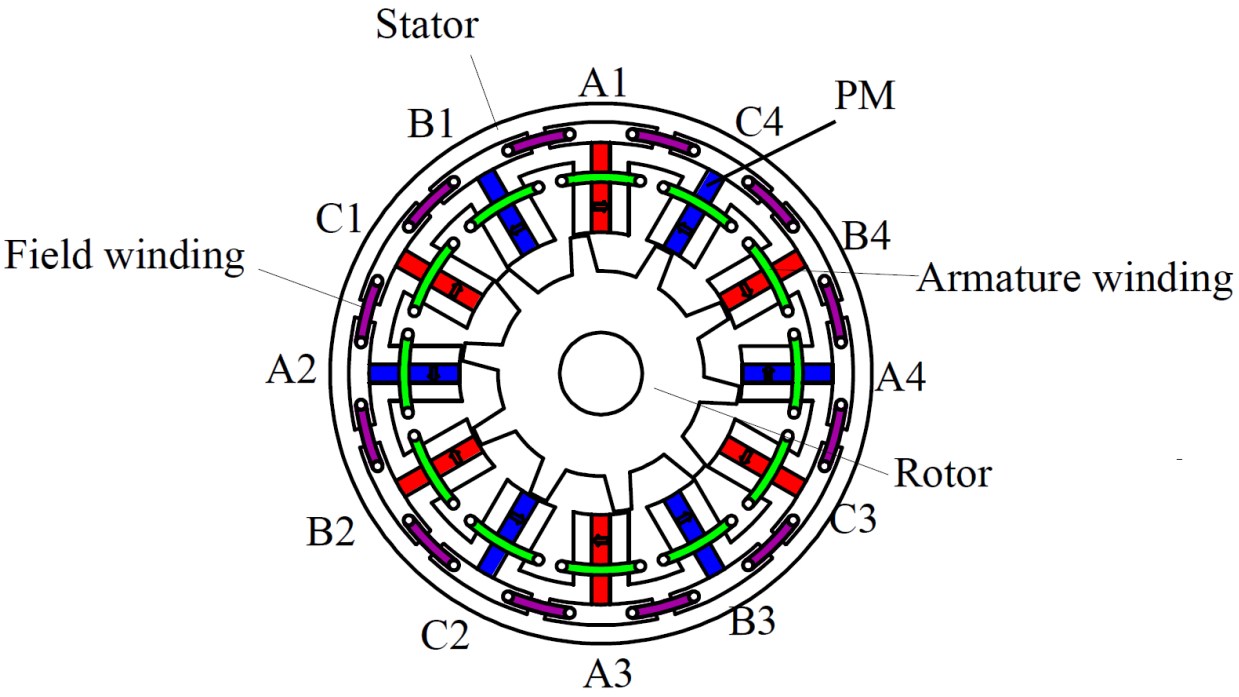
Stator
A1
B1
C4
PM
C1
B4
Field winding
Armature winding
A2
A4
Rotor
B2
C3
C2
B3
A3

Figure 3

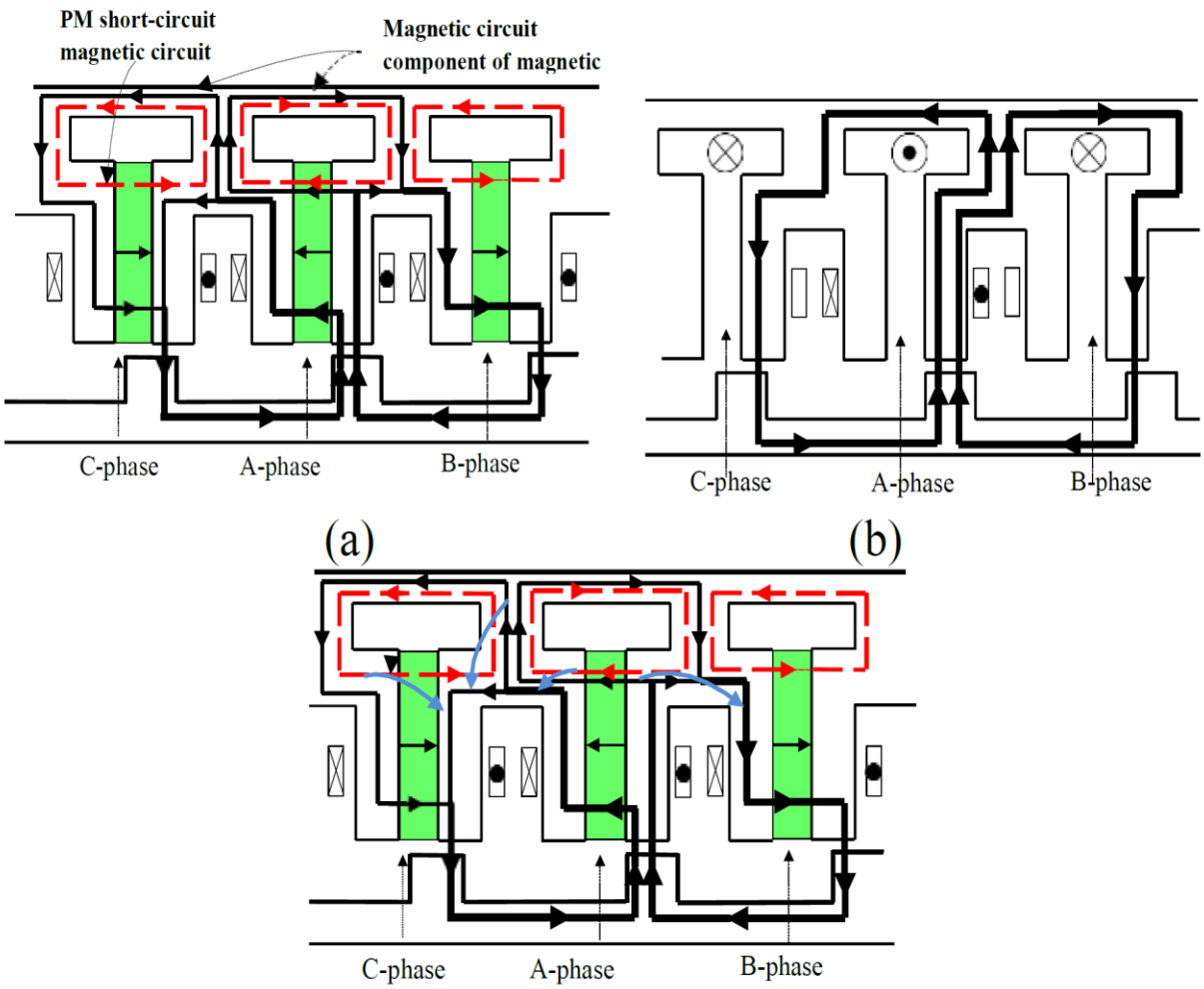
PM short-circuit
magnetic circuit
Magnetic circuit
component of magnetic
C-phase
A-phase
B-phase
(a)
C-phase
A-phase
B-phase
(b)
C-phase
A-phase
B-phase
(c)

Figure 4

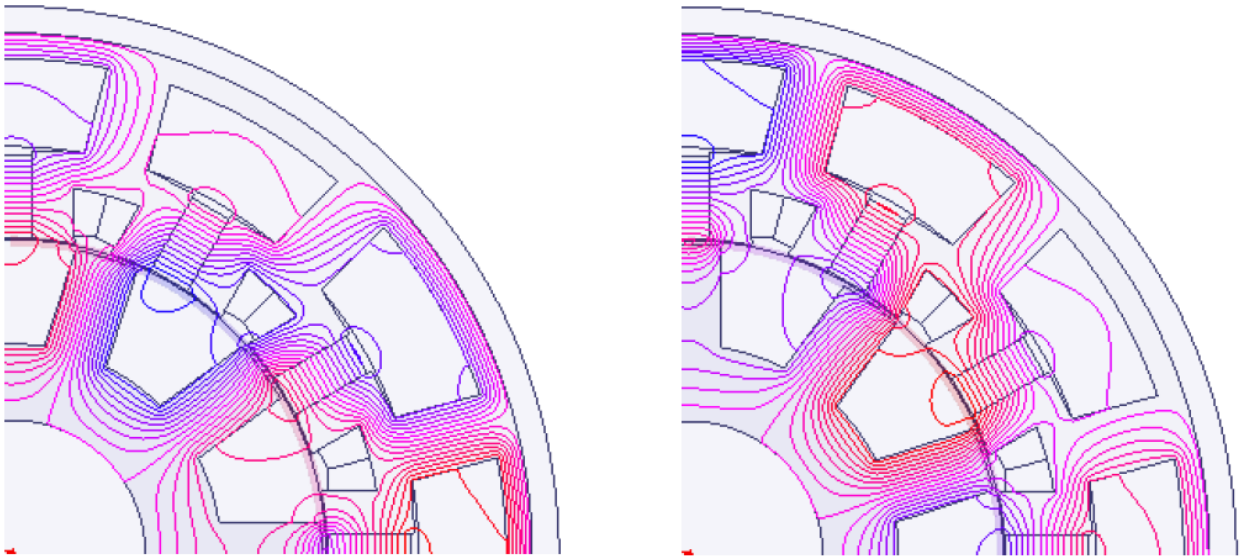

(a) (b)

Figure 5

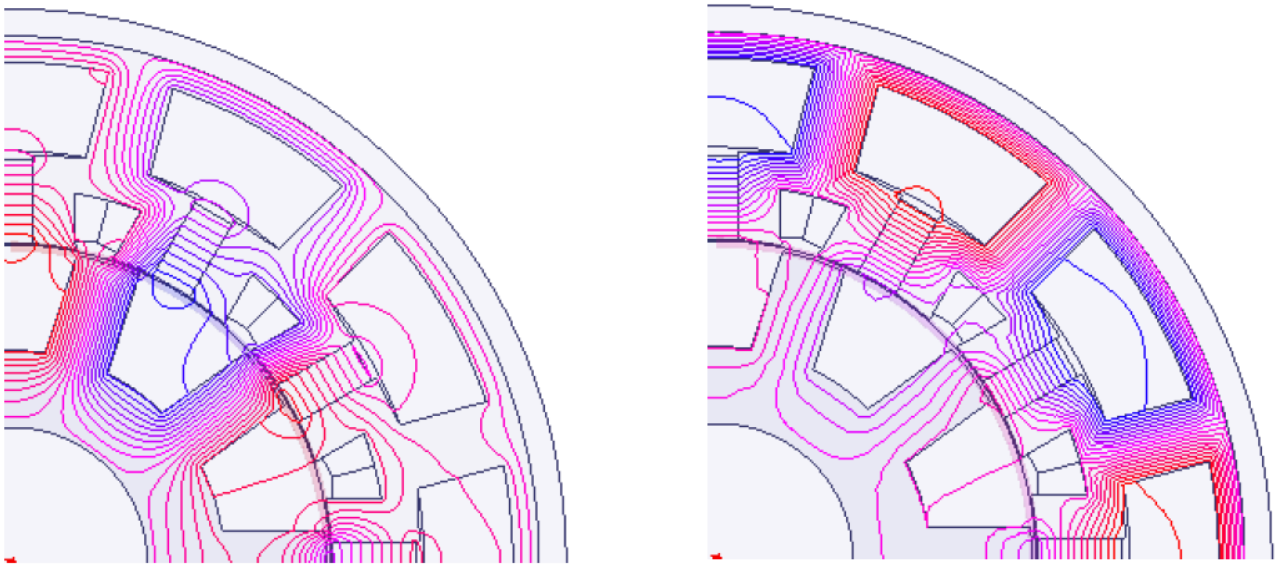

(a) (b)

Figure 6

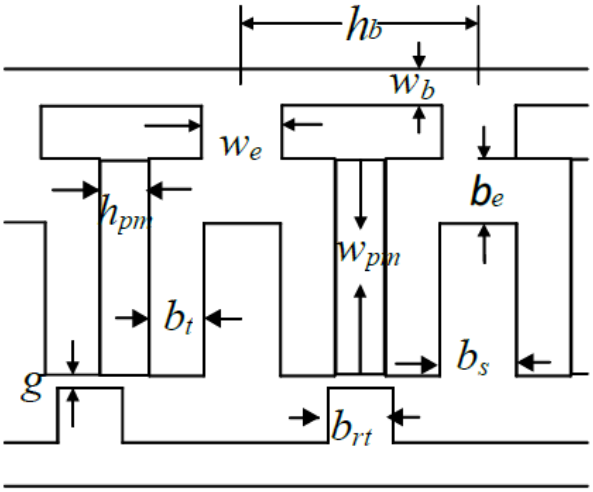

Figure 7

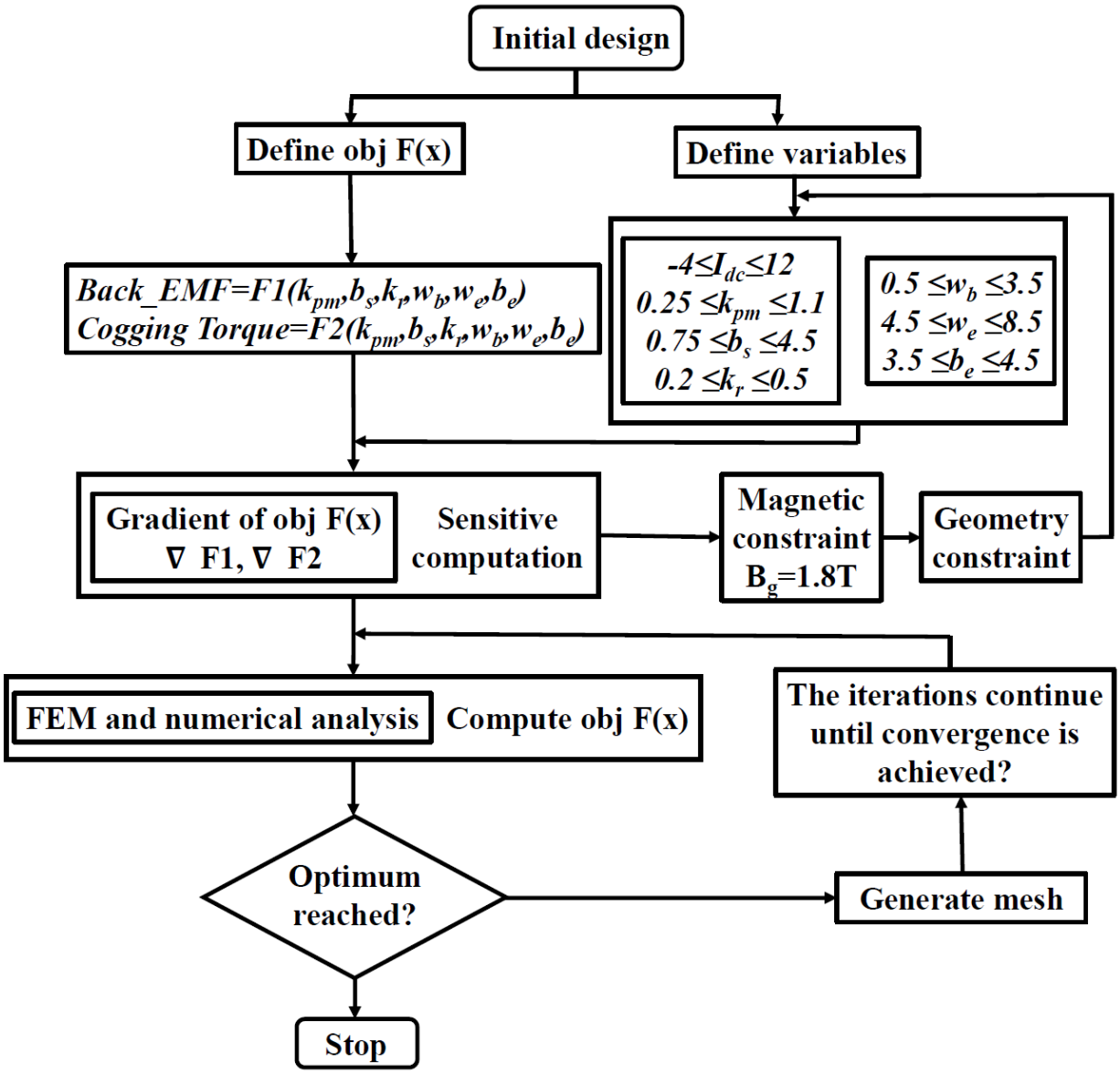
Initial design
Define obj F(x)
Define variables
Back_EMF=F1(k_{pm},b_s,k_r,w_b,w_e,b_e)
Cogging Torque=F2(k_{pm},b_s,k_r,w_b,w_e,b_e)
$-4 \le I_{dc} \le 12$
$0.25 \le k_{pm} \le 1.1$
$0.75 \le b_s \le 4.5$
$0.2 \le k_r \le 0.5$
$0.5 \le w_b \le 3.5$
$4.5 \le w_e \le 8.5$
$3.5 \le b_e \le 4.5$
Gradient of obj F(x)
∇ F1, ∇ F2
Sensitive computation
Magnetic constraint
B_g=1.8T
Geometry constraint
FEM and numerical analysis
Compute obj F(x)
The iterations continue until convergence is achieved?
Optimum reached?
Generate mesh
Stop

Figure 8

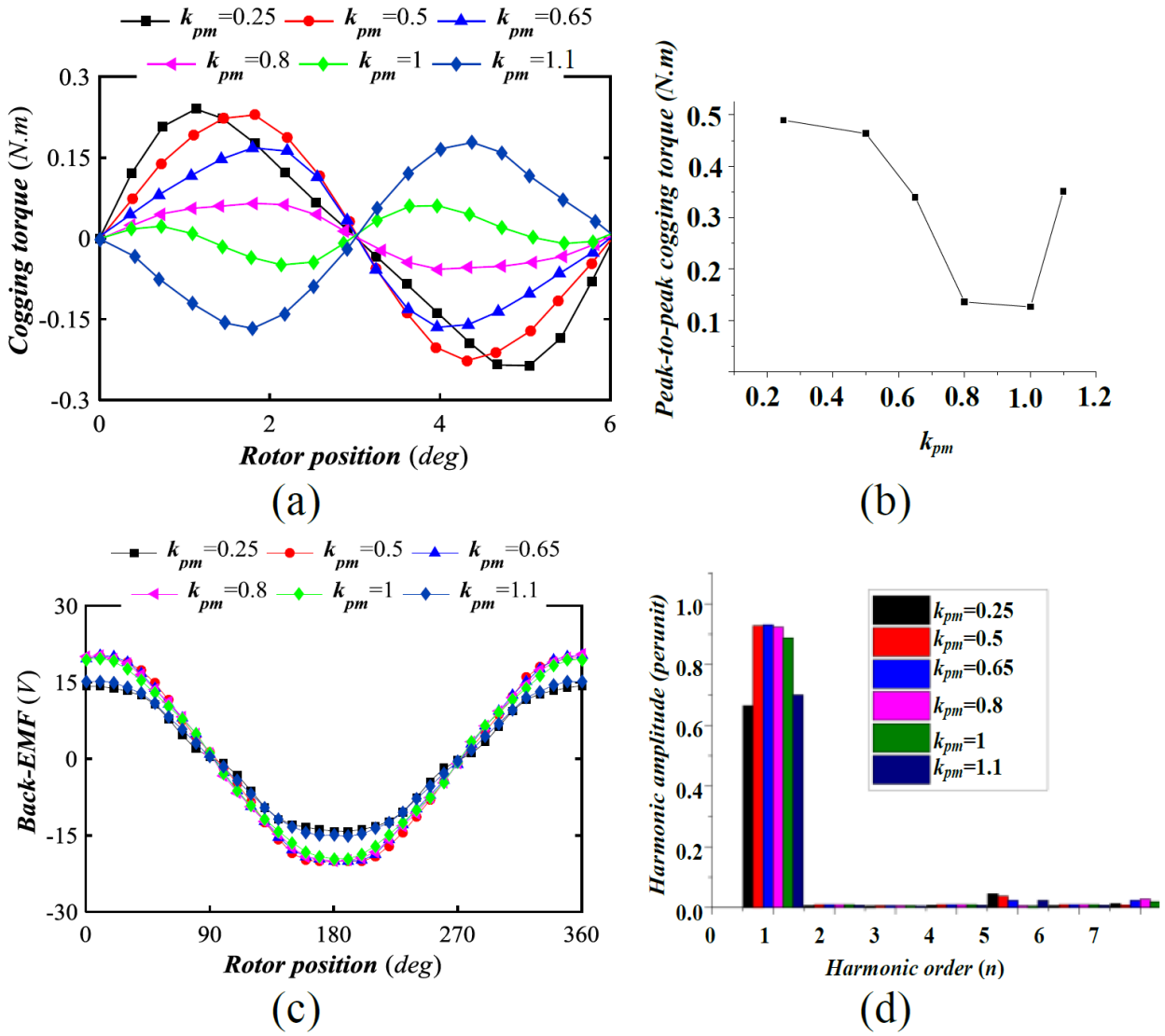
k_{pm}=0.25 k_{pm}=0.5 k_{pm}=0.65
k_{pm}=0.8 k_{pm}=1 k_{pm}=1.1
Cogging torque (N.m)
Rotor position (deg)
(a)
Peak-to-peak cogging torque (N.m)
k_{pm}
(b)
Back-EMF (V)
Rotor position (deg)
(c)
Harmonic amplitude (perunit)
Harmonic order (n)
(d)

Figure 9

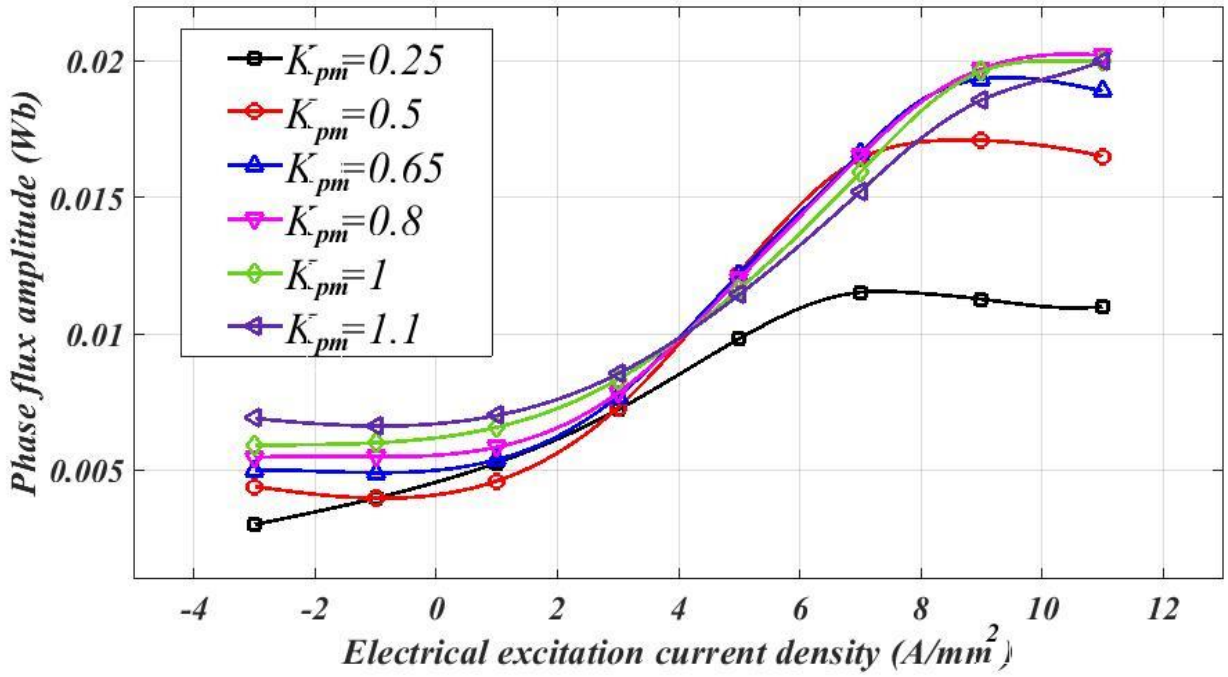
K_{pm}=0.25
K_{pm}=0.5
K_{pm}=0.65
K_{pm}=0.8
K_{pm}=1
K_{pm}=1.1
Phase flux amplitude (Wb)
0.02
0.015
0.01
0.005
-4
-2
0
2
4
6
8
10
12
Electrical excitation current density (A/mm^2)

Figure 10

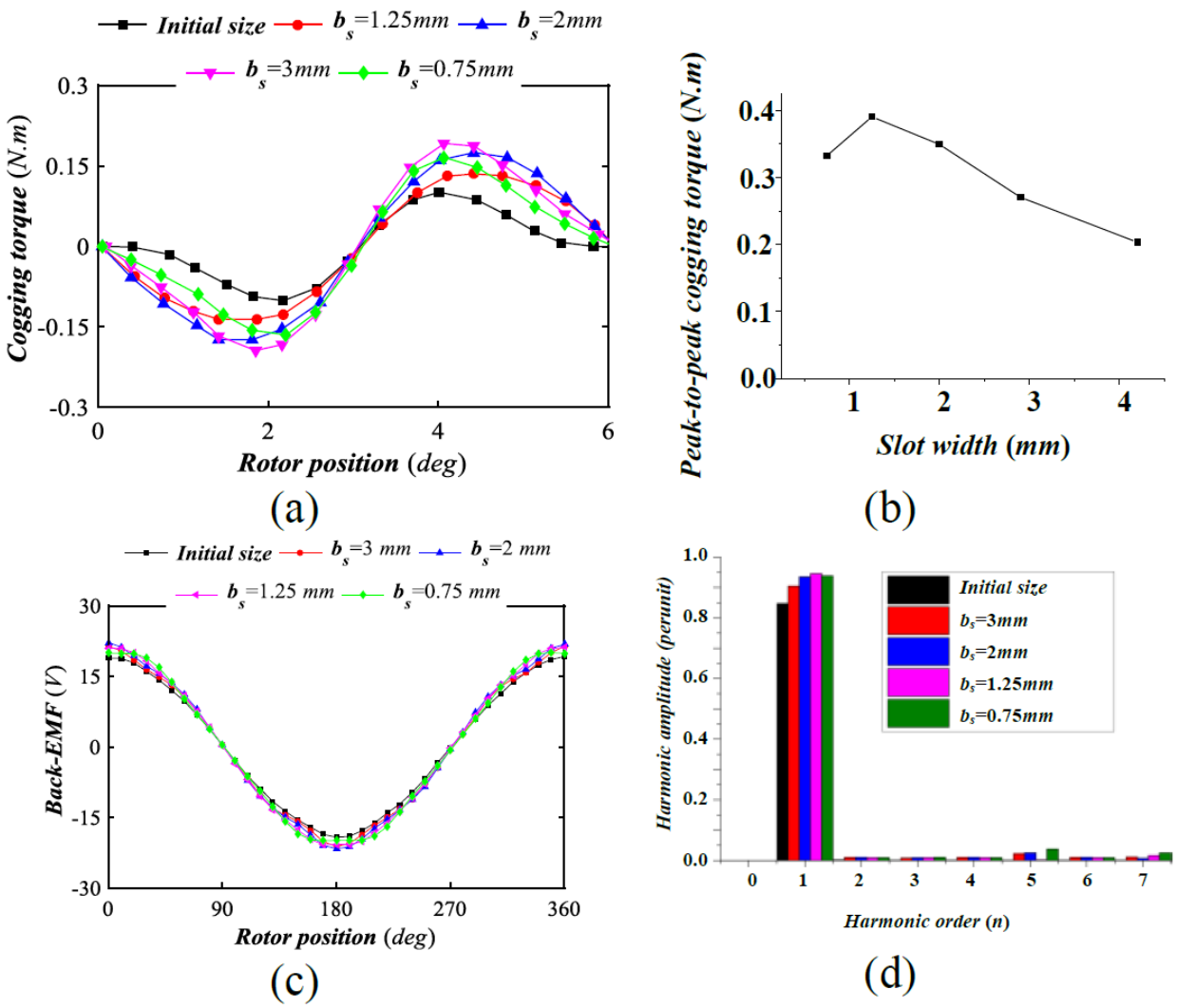
Initial size
b_s=1.25mm
b_s=2mm
b_s=3mm
b_s=0.75mm
Cogging torque (N.m)
Rotor position (deg)
(a)
Peak-to-peak cogging torque (N.m)
Slot width (mm)
(b)
Initial size
b_s=3 mm
b_s=2 mm
b_s=1.25 mm
b_s=0.75 mm
Back-EMF (V)
Rotor position (deg)
(c)
Harmonic amplitude (perunit)
Harmonic order (n)
Initial size
b_s=3mm
b_s=2mm
b_s=1.25mm
b_s=0.75mm
(d)

Figure 11

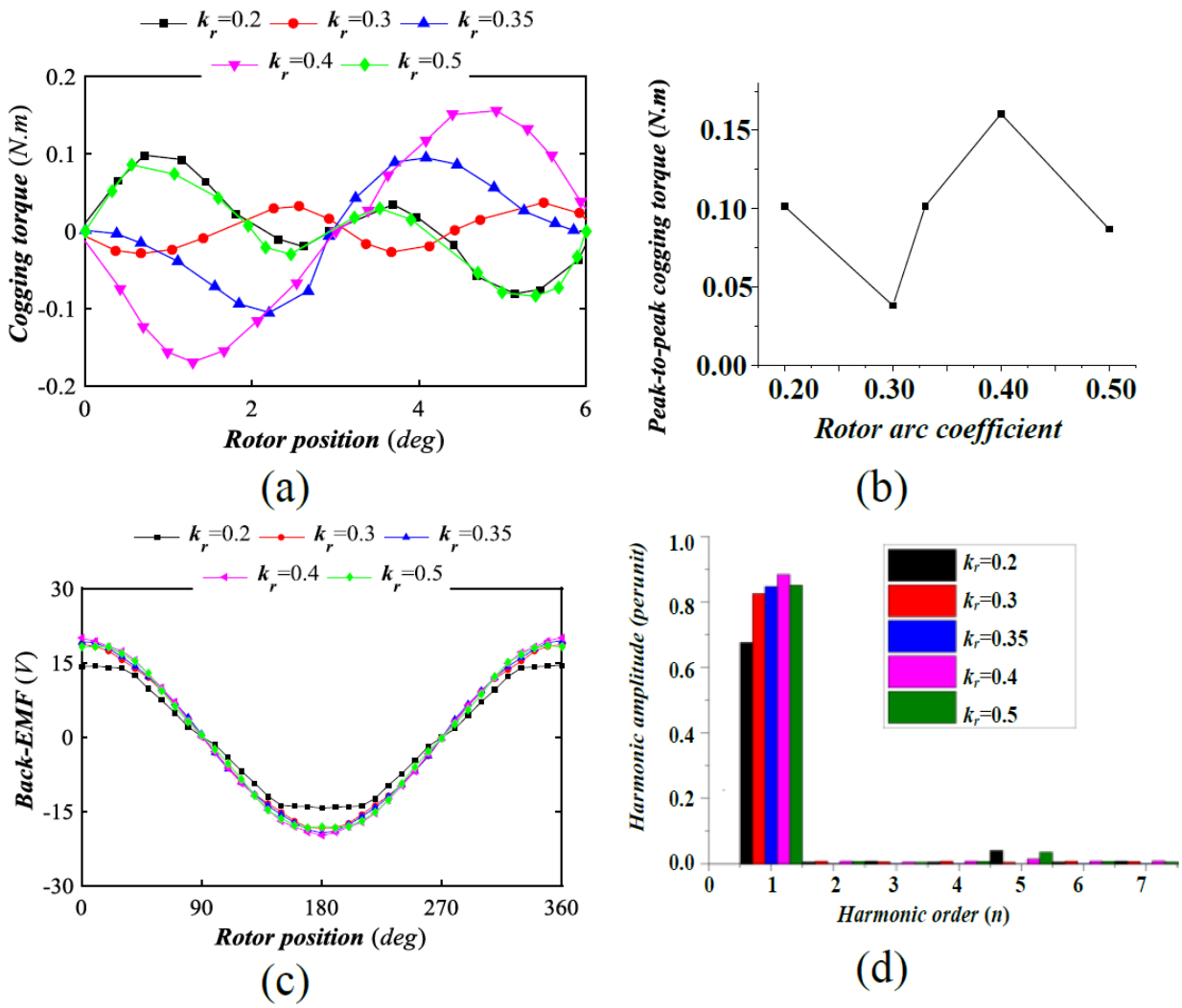
k_r=0.2 k_r=0.3 k_r=0.35
k_r=0.4 k_r=0.5
Cogging torque (N.m)
Rotor position (deg)
(a)
Peak-to-peak cogging torque (N.m)
Rotor arc coefficient
(b)
k_r=0.2 k_r=0.3 k_r=0.35
k_r=0.4 k_r=0.5
Back-EMF (V)
Rotor position (deg)
(c)
Harmonic amplitude (perunit)
Harmonic order (n)
(d)

Figure 12

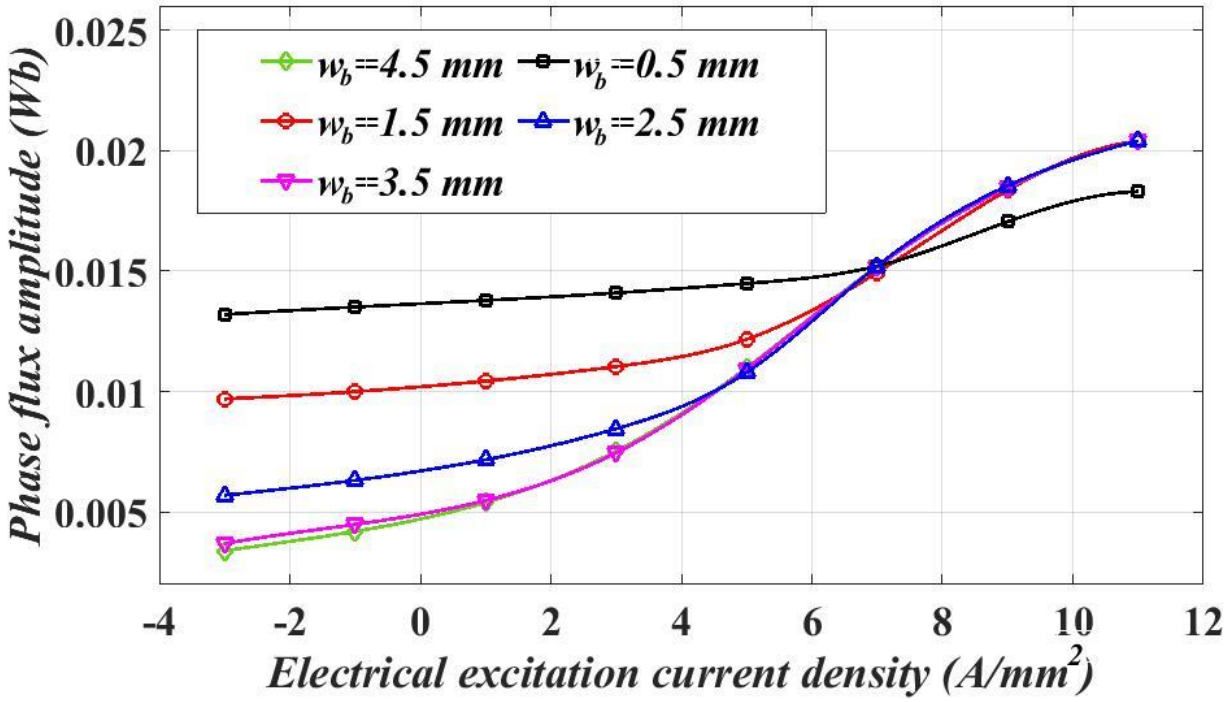
0.025
0.02
0.015
0.01
0.005
Phase flux amplitude (Wb)
w_b==4.5 mm
w_b==0.5 mm
w_b==1.5 mm
w_b==2.5 mm
w_b==3.5 mm
-4
-2
0
2
4
6
8
10
12
Electrical excitation current density (A/mm^2)

Figure 13

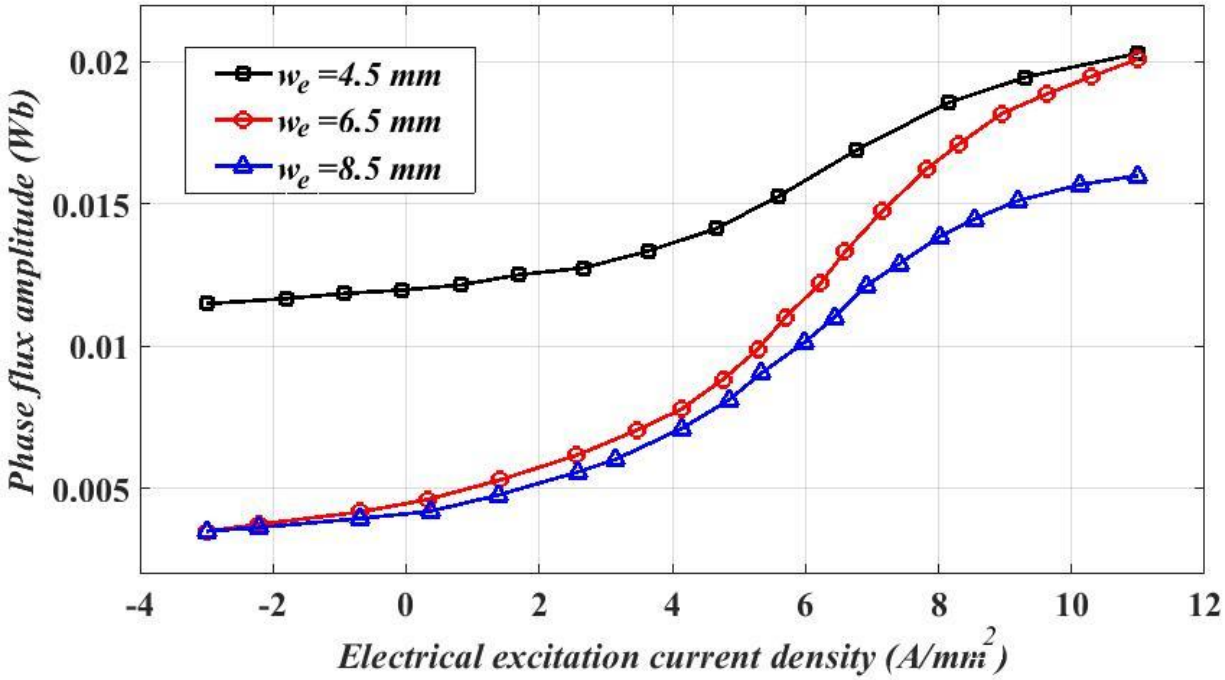
w_e =4.5 mm
w_e =6.5 mm
w_e =8.5 mm
Phase flux amplitude (Wb)
0.02
0.015
0.01
0.005
-4
-2
0
2
4
6
8
10
12
Electrical excitation current density (A/mm^2)

Figure 14

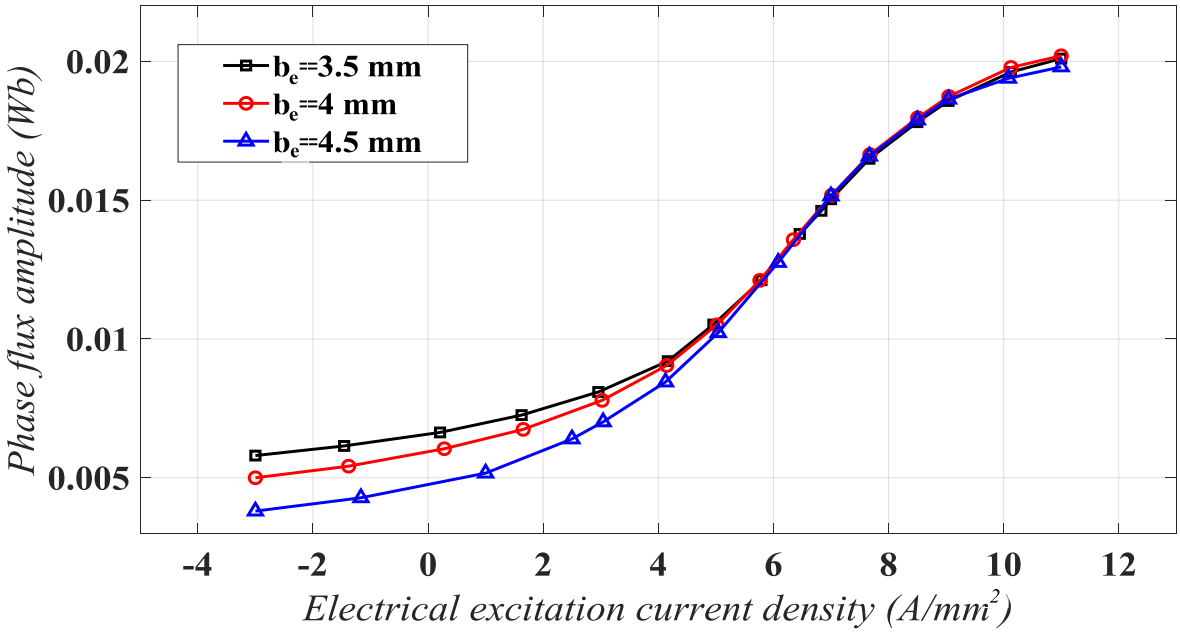
b_e==3.5 mm
b_e==4 mm
b_e==4.5 mm
0.02
0.015
0.01
0.005
Phase flux amplitude (Wb)
-4
-2
0
2
4
6
8
10
12
Electrical excitation current density (A/mm²)

Figure 15

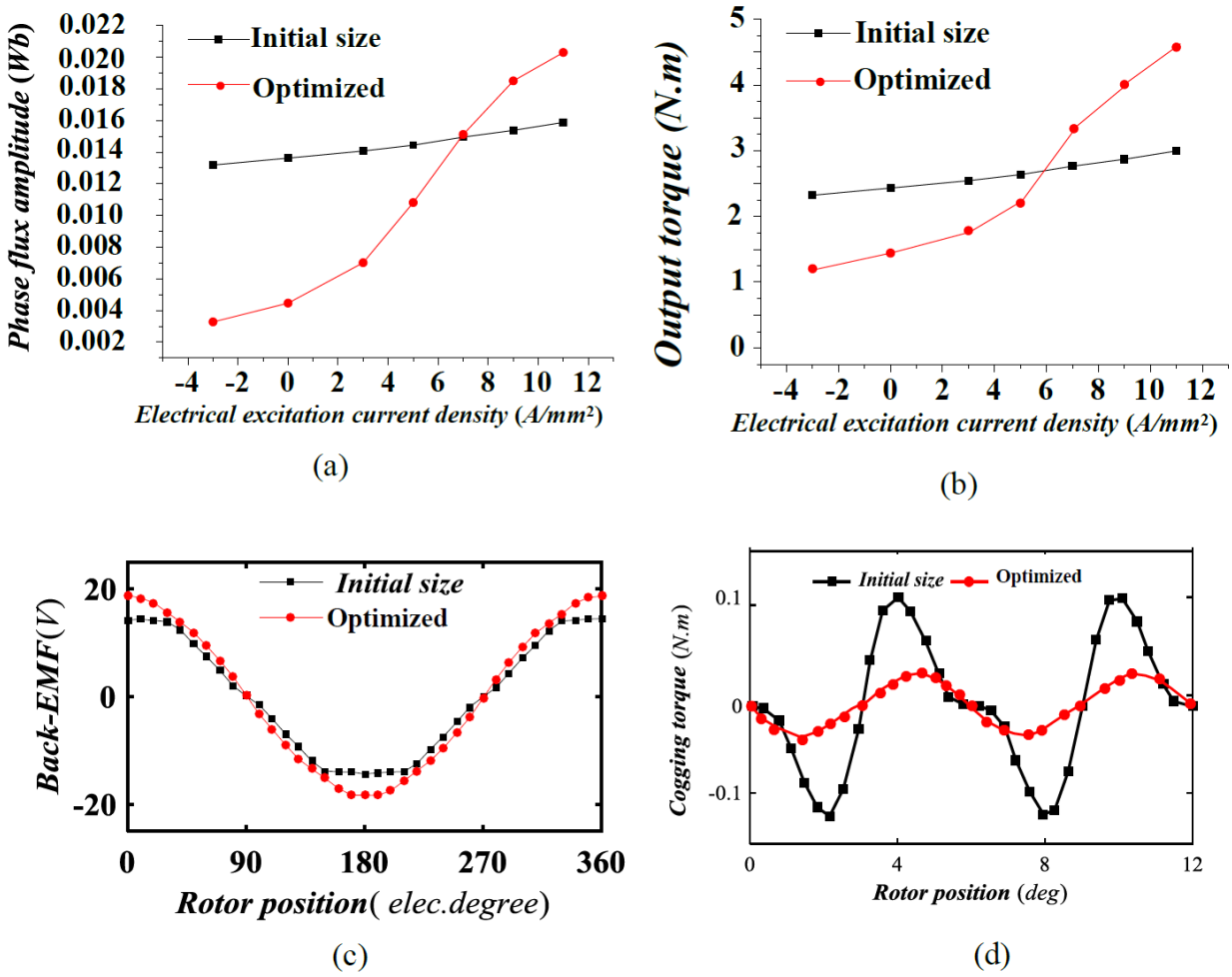
Phase flux amplitude (Wb)
0.022
0.020
0.018
0.016
0.014
0.012
0.010
0.008
0.006
0.004
0.002
Initial size
Optimized
-4 -2 0 2 4 6 8 10 12
Electrical excitation current density (A/mm²)
(a)
Output torque (N.m)
5
4
3
2
1
0
Initial size
Optimized
-4 -2 0 2 4 6 8 10 12
Electrical excitation current density (A/mm²)
(b)
Back-EMF(V)
20
0
-20
Initial size
Optimized
0 90 180 270 360
Rotor position(elec.degree)
(c)
Cogging torque (N.m)
0.1
0
-0.1
Initial size
Optimized
0 4 8 12
Rotor position (deg)
(d)

Figure 16

(a)

(b)

(c)

Figure 17

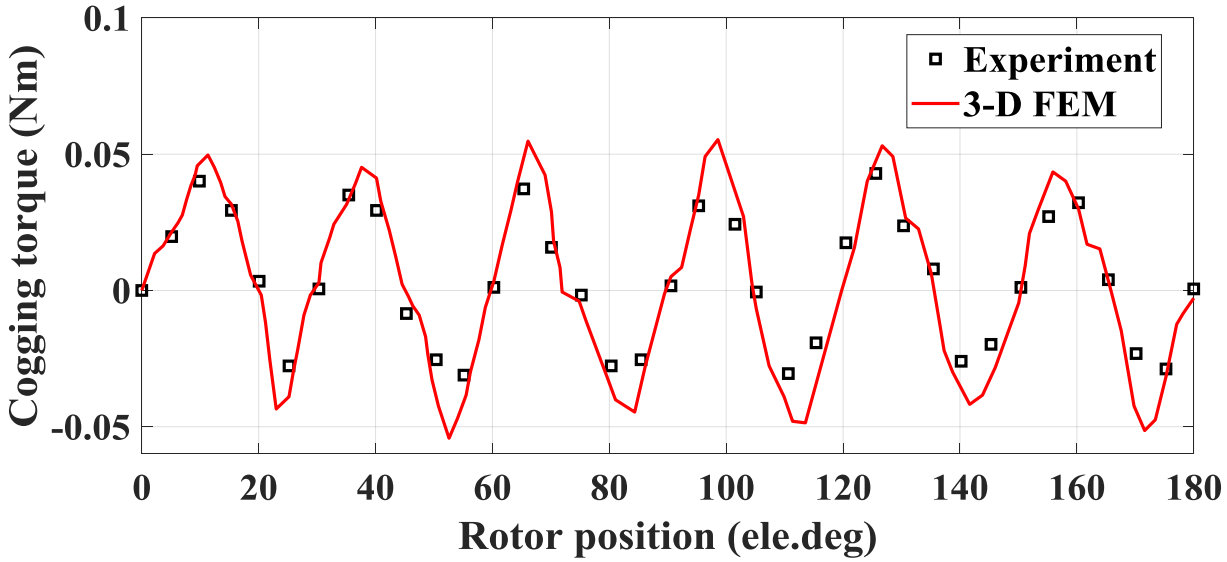

Figure 18

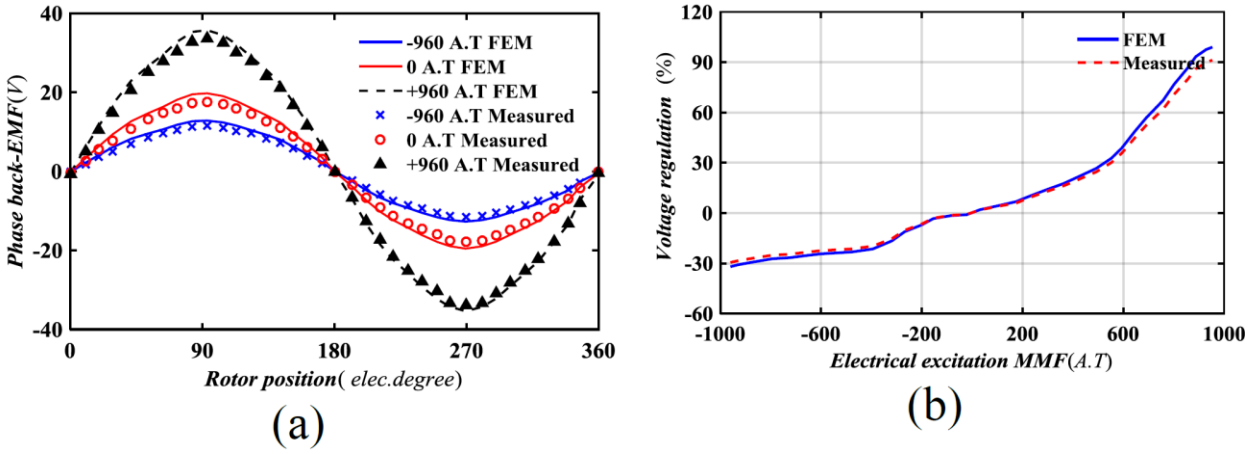

Figure 19

Table 1

Rated speed (r/min)	Rated power (W)	Bus voltage (V-DC)	Peak rated current (A)
1200	500	48	20

Table 2

Variable	Symbol	Initial value	Constraint
PM thickness	$k_{pm} = \frac{\theta_{pm}}{\theta_{pm-ort}}$	1	$[0.25,1.1]$
Stator slot width	b_s	4.1 mm	$[0.75,4.5]$mm
Rotor pole width	$k_r = \frac{b_r}{\pi D_a / N_r}$	0.33	$[0.2,0.5]$
Magnetic bridge width	W_b	2.5 mm	$[0.5,3.5]$mm
The core width in the middle of excitation slot	W_e	6.3 mm	$[4.5,8.5]$mm
Stator yoke width	b_e	4 mm	$[3.5,4.5]$mm

Table 3

Variable	Initial value	Optimized
PM thickness	1	0.8
Stator slot width	4.1 mm	1.25
Rotor pole width	0.33	0.4
Magnetic bridge width	2.5 mm	3.5
The core width in the middle of excitation slot	6.3 mm	6.5
Stator yoke width	4 mm	4.5

Table 4

Performance	Initial design	Optimal design
D-axis inductance	1.01 mH	1.08 mH
Q-axis inductance	1.07 mH	1.15 mH
Efficiency	89.65%	92.45%
Power factor	0.65	0.71